Dynamical Mountain Meteorology

Dr. Yuh-Lang Lin, ylin@cat.edu; http://mesolab.org
Department of Physics/Department of Energy & Environmental Systems
North Carolina A&T State University
(Ref.: *Mesoscale Dynamics*, Y.-L. Lin, Cambridge, 2007)

Chapter 6 Reflection and Critical Levels

(Based on Sec. 3.7&3.8 of "Mesoscale Dynamics" (2007, Cambridge) by Y.-L. Lin)
(classical equation editor: $c_p \neq f(k)$)

3.7 Wave reflection levels

- Atmospheric waves may be reflected from the Earth's surface, the surface of a fluid, or the internal interface at density discontinuity.

- If the atmospheric structure, such as the Brunt-Vaisala frequency (N) and the basic wind velocity (U), varies with height, then gravity waves may be reflected from and/or transmitted through the interface at which rapid changes in atmospheric structure occur.

- In order to help understand the basic properties of wave reflection and transmission, we consider a simple fluid system similar to that for pure gravity waves [(3.5.5)], except that the fluid is now comprised of two layers, each with different buoyancy frequencies (N_1 and N_2 in the lower and upper layers, respectively; see Fig. 3.11).

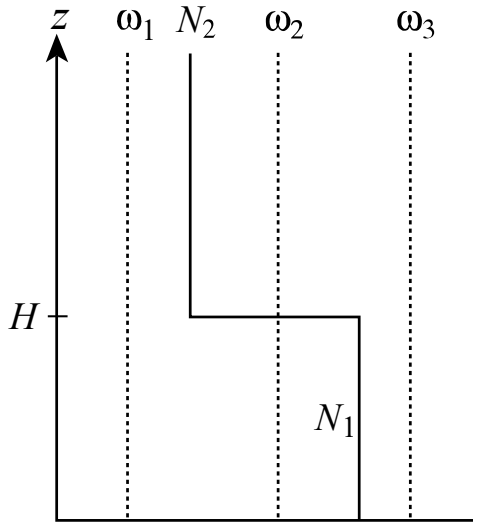

Fig. 3.11: Examples of wave reflection in a stratified flow with a piecewise constant profile in Brunt-Vaisala frequency (N). Case ω_1 has wave solutions in both layers; Case ω_2 has wave solutions in the lower layer, evanescent solutions in upper layer; and Case ω_3 has evanescent solutions in both layers. The forcing is assumed at $z = 0$.

- We further assume that there is no basic flow ($U = 0$). Under these constraints, the governing equations for the small-amplitude vertical velocities w_1' and w_2' in each layer of this particular two-dimensional fluid system may be written as

$$\frac{\partial^2}{\partial t^2}\left(\frac{\partial^2 w_1'}{\partial x^2}+\frac{\partial^2 w_1'}{\partial z^2}\right)+N_1^{\,2}\frac{\partial^2 w_1'}{\partial x^2}=0, \quad 0\le z<H, \qquad (3.7.1)$$

$$\frac{\partial^2}{\partial t^2}\left(\frac{\partial^2 w_2'}{\partial x^2}+\frac{\partial^2 w_2'}{\partial z^2}\right)+N_2^{2}\frac{\partial^2 w_2'}{\partial x^2}=0, \quad H\le z. \qquad (3.7.2)$$

- Applying the method of normal modes,

  $w' = \hat{w}(z)\exp[i(kx - \omega t)]$,

  to the above equations leads to the following equations for the vertical structure in each layer:

$$\frac{\partial^2 \hat{w}_1}{\partial z^2} + m_1^2 \hat{w}_1 = 0, \quad 0 \le z < H, \tag{3.7.3}$$

$$\frac{\partial^2 \hat{w}_2}{\partial z^2} + m_2^2 \hat{w}_2 = 0, \quad H \le z, \tag{3.7.4}$$

  where

$$m_i^2 = k^2\left(N_i^2/\omega^2 - 1\right), \quad i = 1,2. \tag{3.7.5}$$

- In fact, (3.7.5) represents the dispersion relationships in each layer, which are identical to (3.5.12) if m is replaced by m_i.

  Note that in the above equation (3.7.5), we have assumed that the wave frequencies (ω) and wavenumber (k) are identical in each layer. This simple type of piecewise layered model is able to provide the fundamental wave dynamics.

- It can be shown that the following solutions satisfy (3.7.3) and (3.7.4),

$$\hat{w}_1 = A\, e^{im_1(z-H)} + B\, e^{-im_1(z-H)}, \quad 0 \le z < H \tag{3.7.6}$$

$$\hat{w}_2 = C\, e^{im_2(z-H)} + D\, e^{-im_2(z-H)}, \quad H \le z\,. \tag{3.7.7}$$

- Similar to the one-layer theory discussed in the previous section, the flow response is quite different depending on whether m_i, $i = 1, 2$, is real or imaginary (i.e. whether $N > \omega$ or $N < \omega$).

- If we assume a less stable layer sitting on top of a more stable layer ($N_2 < N_1$), then this leads to three possible cases:

  (a) $N_i > \omega$ for $i = 1, 2$;

  (b) $N_i < \omega$ for i=1, 2; or

  (c) $N_2 < \omega < N_1$ (as shown in Fig. 3.11).

  This situation $N_2 < N_1$ may occur in the vicinity of a thunderstorm in which the lower layer is more stable due to the evaporative cooling associated with rainfall.

  The opposite situation, ($N_2 > N_1$), often occurs when a mixed boundary layer is produced by surface sensible heating during the day, or when the stratosphere is considered in the problem, when N_2 is normally two to three times larger than N_1.

- In the following, we will restrict our attention to the case with $N_2 < \omega < N_1$ (i.e. Case ω_2 of Fig. 3.11). Solutions for other cases may be obtained in a similar manner. The lower boundary condition for flow over a flat surface requires that the normal velocity component vanish, i.e. $w' = 0$ at $z = 0$.

  Applying this lower boundary condition to (3.7.6) yields

$$\hat{w}_1 = B\left[e^{-im_1(z-H)} - e^{2im_1H}e^{im_1(z-H)}\right], \quad 0 \le z < H\,. \tag{3.7.8}$$

- In the above equation, the first term inside the square bracket represents waves with upward energy propagation, while the second term represents waves with downward energy propagation, since $z - H$ is negative. If the wave energy source is located at the surface, then the absolute value of $\exp(2im_1H)$ represents the reflection coefficient. In the upper layer, since m_2 is imaginary, (3.7.7) becomes

$$\hat{w}_2 = C\,e^{-n_2(z-H)} + D\,e^{n_2(z-H)}, \quad H \le z, \tag{3.7.9}$$

  where $n_2 = im_2 = k\sqrt{1 - N_2^2/\omega^2}$ is a real number.

- For a wave energy source located in the lower layer, the upper boundary condition requires a bounded solution, which, in turn, requires that $D = 0$. Thus, (3.7.7) reduces to

$$\hat{w}_2 = C\,e^{-n_2(z-H)}, \qquad H \le z\,. \tag{3.7.10}$$

- The above equation represents evanescent waves, as described in Section 3.5.

  However, for cases with real values of m_2, the upper boundary condition is governed by the radiation boundary condition, which will be discussed in Section 4.4. Therefore, the radiation condition requires that $D = 0$ if the wave energy source is located in the lower layer. Coefficients B and C are determined by boundary conditions at the interface, i.e. by imposing the appropriate kinematic and dynamic boundary conditions at $z = H$.

  The kinematic boundary condition requires that

$$\boldsymbol{V}_1 \cdot \boldsymbol{n}_1 = \boldsymbol{V}_2 \cdot \boldsymbol{n}_2 , \tag{3.7.11}$$

  where the subscripts indicate the upper or lower layer; $\boldsymbol{V}_i$ is the total velocity in layer i; and $\boldsymbol{n}_i$ is the unit vector normal to the boundary in each layer. Note that $\boldsymbol{n}_i$ in (3.7.11) is a vector, which should not be confused with the n_i used in (3.7.9) and (3.7.10).

  For a small-amplitude (linear) perturbation, the unit normal vector is almost vertical since the wave amplitude is much smaller than the wavelength. This then implies that

$$w'_1 = w'_2 . \tag{3.7.12}$$

Another interface boundary condition is the dynamic boundary condition specifying continuity of pressure at $z = H$, i.e. $p'_1 = p'_2$, which leads to

$$\frac{\partial w'_1}{\partial z} = \frac{\partial w'_2}{\partial z} . \qquad (3.7.13)$$

- Applying (3.7.12) to (3.7.8) and (3.7.10) at $z = H$ gives

$$\hat{w}_1 = \frac{C}{1 - e^{-2im_1 H}} \left[e^{im_1 (z-H)} - e^{-2im_1 H} e^{-im_1 (z-H)} \right], \; 0 \le z < H . \qquad (3.7.14)$$

- Applying the dynamic boundary condition, (3.7.13), to (3.7.14) and (3.7.10) yields the dispersion relationship for this two-layer fluid system,

$$e^{-2im_1 H} = \frac{n_2 + im_1}{n_2 - im_1} . \qquad (3.7.15)$$

This expression may also be used to find the eigenvalues, ω and k, which are needed for substitution into (3.7.15) in order to obtain the eigenfunctions that describe the vertical structure of the wave,

$$\hat{w}_1 = C \left[\left(\frac{m_1 + in_2}{2m_1} \right) e^{im_1 (z-H)} + \left(\frac{m_1 - in_2}{2m_1} \right) e^{-im_1 (z-H)} \right] . \qquad (3.7.16)$$

The reflection coefficient for a forcing located at the surface ($z = 0$) and the wave being reflected at $z = H$ may be obtained by taking the absolute value of the ratio of the first term (term A) to the second term (term B) inside the square bracket of the above equation, which gives the reflection coefficient $r = \left|(m_1 + in_2)/(m_1 - in_2)\right|$. Note that $z - H$ is negative in the lower layer.

- In addition to interfacial discontinuities in stratification, wave reflection may also occur when the vertical profiles of the basic state wind and the stratification (Brunt-Vaisala frequency) vary continuously throughout the fluid (Fig. 3.12).

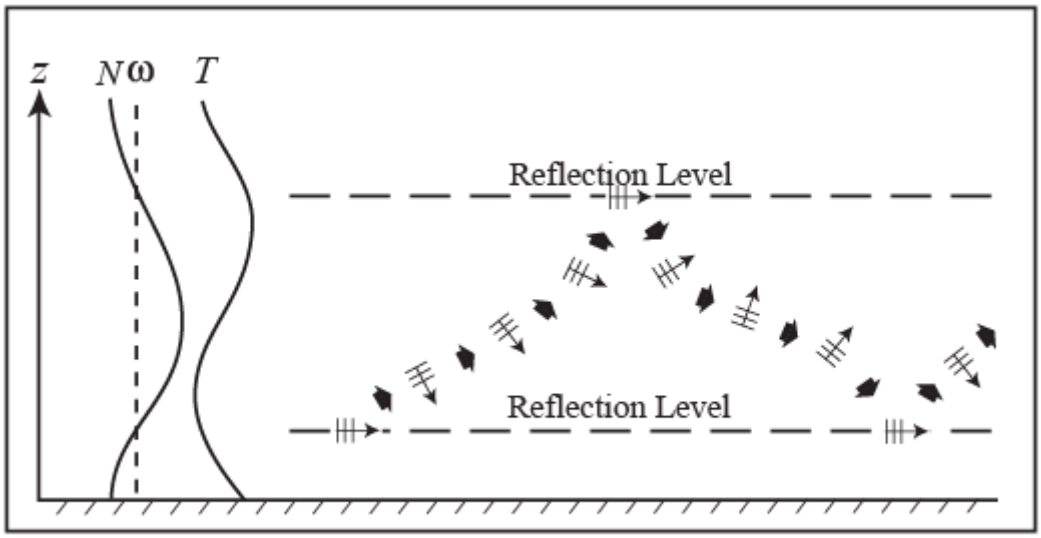

Fig. 3.12: Wave reflection in a continuously stratified fluid. N and T are the Brunt-Vaisala frequency and temperature of the sounding, respectively, and ω is the wave frequency. Ray paths are reflected at the reflection level at which $\omega = N$. A wave packet is also depicted in the figure. The short blunt arrows and long thin arrows denote the group and phase velocities, respectively, of the wave packet. Particle motions are parallel to the constant phase lines or wave fronts, which become vertically oriented at the reflection level since α, defined in (3.5.13) and also illustrated in Fig. 3.9, approaches 0. (After Lin 2007; Adapted after Hooke 1986)

- To elucidate this further, we consider a two-dimensional, linear, nonrotating, inviscid, Boussinesq fluid system governed by (3.5.1) - (3.5.4), but whose basic state is generalized, to allow for both the background wind and Brunt-Vaisala frequency to vary with height. The equation governing this special type of fluid system may also be derived directly from the generalized linear equation set, (2.2.14) - (2.2.18) and is given by

$$\frac{\partial^2 \hat{w}}{\partial z^2} + m^2(z)\hat{w} = 0\,, \tag{3.7.17}$$

where

$$m^2(z) = \frac{N^2}{(U-c)^2} - \frac{U_{zz}}{U-c} - k^2\,,\quad c = \frac{\omega}{k}\,. \tag{3.7.18}$$

- Equation (3.7.17) is a reduced form in the wave-number space of the *Taylor-Goldstein equation*,

$$\frac{D^2}{Dt^2}\nabla^2 w' - U_{zz}\frac{D}{Dt}\left(\frac{\partial w'}{\partial x}\right) + N^2\frac{\partial^2 w'}{\partial x^2} = 0\,. \tag{3.7.19}$$

Note that m in (3.7.18) can be viewed as the vertical wave number, and the solutions of (3.7.17) can be written in the form of $\exp(\pm imz)$ when U and N are constant. If m^2 changes sign from positive to negative at a certain level, then m^2 will change from a real to an imaginary number. A transition from the vertically propagating wave regime to the evanescent flow

regime occurs based on an argument similar to that given for the solutions of (3.5.8) and (3.5.9).

If a vertically propagating wave-like disturbance exists below that particular level, such as $z = H$ for ω_2 of Fig. 3.11, it will exponentially decay above that level. In this situation, the wave energy is not able to freely propagate vertically above $z = H$ and is therefore forced to reflect back. This level is called the *wave reflection level*.

If such a reflection level exists above the lower, rigid, flat surface, this atmospheric layer then acts as a wave guide in trapping the wave energy between the reflection level and the surface and allows for the wave energy to effectively propagate far downstream horizontally.

- One well-known example of gravity wave reflection in the atmosphere is the lee waves (Section 5.2) generated by stratified airflow over a two-dimensional mountain ridge when the stratification (wind speed) is much stronger (smaller) in the lower layer compared to the upper layer.

The idea of wave reflection in a slow-varying density gradient or stratification may also be traced by the paths of rays, whose directions (α) are defined locally by (3.5.13), as shown by the long-thin arrows in Fig. 3.12.

Ray paths are defined as paths where the tangent at any one point is in the direction of the group velocity (relative to the ground) of the waves. When a group of waves approaches the reflection level where $\omega = N$, α approaches 0, and the wave fronts are turned towards the vertical, reflecting the wave energy.

3.8 Critical levels

- Another important phenomenon associated with gravity waves is the change in wave properties across a critical level.

- Note that the equation governing the vertical structure (3.7.17)

$$\frac{\partial^2 \hat{w}}{\partial z^2} + m^2(z)\hat{w} = 0\,, \qquad (3.7.17)$$

where

$$m^2(z) = \frac{N^2}{(U-c)^2} - \frac{U_{zz}}{U-c} - k^2\,, \quad c = \frac{\omega}{k}\,. \qquad (3.7.18)$$

has a singularity when U=c.

- A *critical level* (z_c) is defined as the level at which the vertically sheared basic flow $U(z)$ is equal to the horizontal phase speed (c) of the wave or disturbance, i.e. $U(z_c) = c$.

From an observational analysis of the Oklahoma squall line as depicted in Fig. 6.12 (Chapter 6), there exists a critical level near 6 km. Climatological studies indicate that most midlatitude squall lines exhibit a critical level in the mid-troposphere (Bluestein and Jain 1985; Wyss and Emanuel 1988).

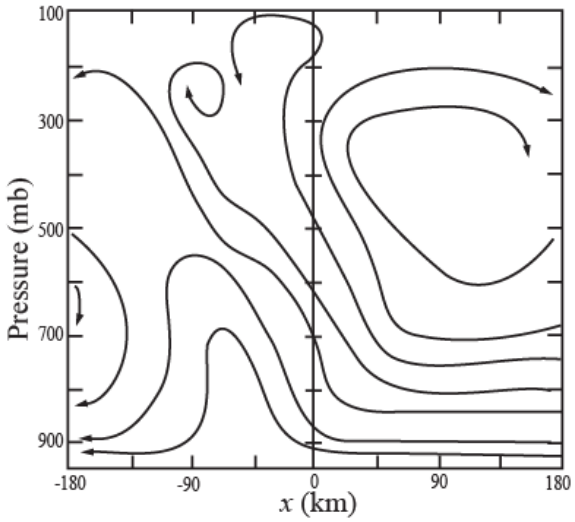

Fig. 6.12: Streamlines relative to a midlatitude squall line observed on 22 May 1976 in the vertical plane with *x* representing distance ahead of the leading edge of the squall line. Three important features are shown: (a) upshear tilt of the updraft, (b) downdraft fed by the front-to-rear flow, and (c) flow overturning in the middle layer. (From Ogura and Liou 1980)

- Nonlinear numerical simulations indicate that a high-drag or severe-wind state may be established after the upward propagating wave breaks above the mountain.

  The wave-breaking region is characterized by strong turbulent mixing with a local wind reversal on top of it.

  Note that the critical level coincides with the wind reversal level for a stationary mountain wave because the phase speed there is zero.

  The wave breaking region aloft might act as an internal boundary that reflects the upward propagating waves back to

the ground and produces a high-drag state through partial resonance with the upward propagating mountain waves, as will be discussed in Ch. 5.

One example of the wave-induced critical level simulated by a numerical model is given in Figs. 5.9 and 5.10 (Chapter 5).

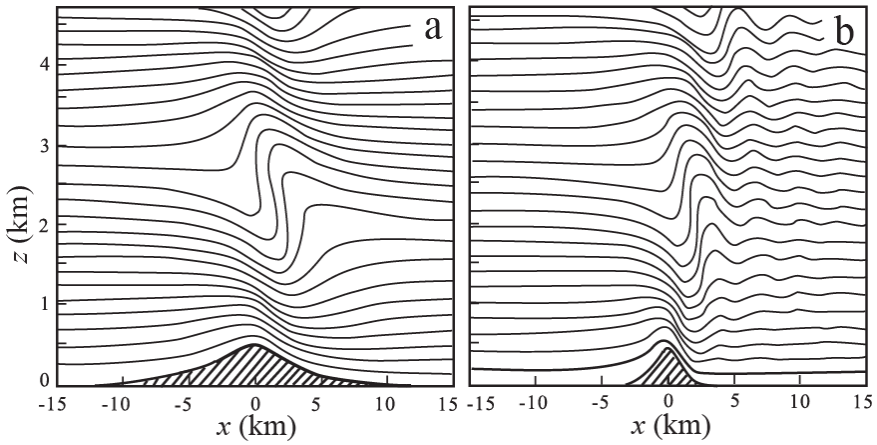

Fig. 5.9: (a) Streamlines for Long's model solution over a bell-shaped mountain with $U = 5$ ms^{-1}, N = 0.01 s^{-1}, $h_m = 500$ m and $a = 3$ km; and (b) same as (a) except with $a = 1$ km. An iterative method is adopted in solving the nonlinear equation (5.3.2) with the nonlinear lower boundary condition (5.3.3) applied. Note that the dispersive tail of the nonhydrostatic waves is present in the narrower mountain (case (b)). (Adapted from Laprise and Peltier 1989a)

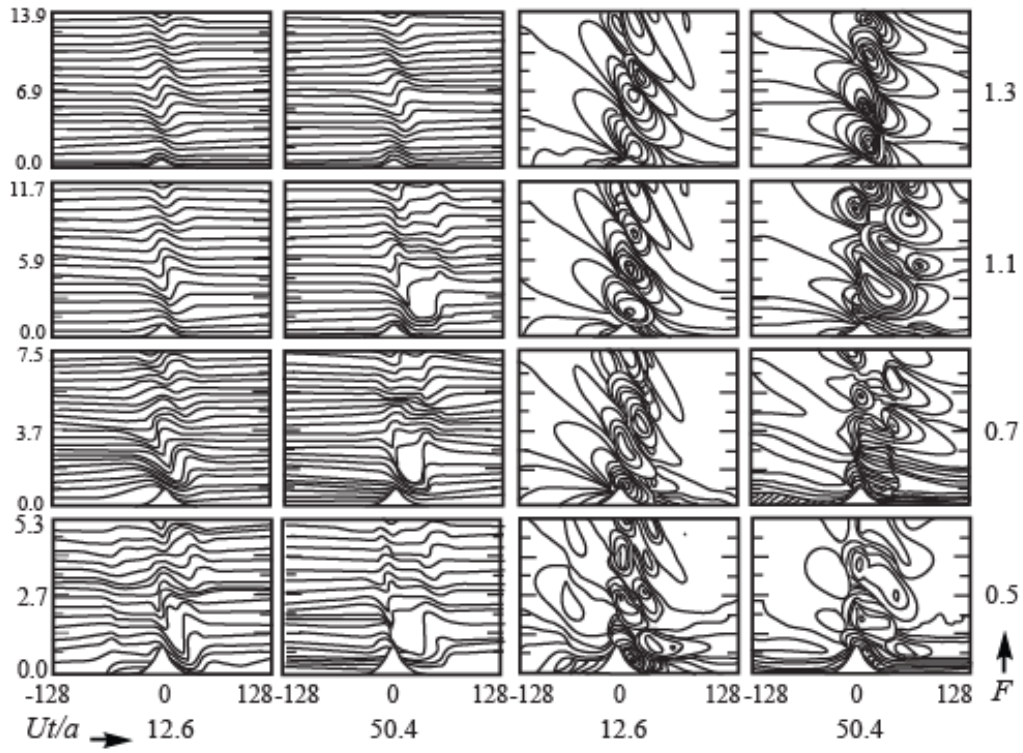

Fig. 5.10: Nonlinear flow regimes for a two-dimensional, hydrostatic, uniform flow over a bell-shaped mountain as simulated by a numerical model, based on the Froude number ($F = U / Nh$). F varies from 0.5 to 1.3, which gives four different flow regimes as discussed in the text. Displayed are the θ fields (left two columns) and the u' fields (right two columns) for two nondimensional times $Ut / a = 12.6$ and 50.4. The dimensional parameters are: $N = 0.01$ ms^{-1}, h = 1 km, a = 10 km, and U = 5, 7, 11, and 13 ms^{-1} correspondig to F = 0.5, 0.7, 1.1, and 1.3, respectively. A constant nondimensional physical domain height of $1.7\lambda_z$ (where $\lambda_z = 2\pi U / N$) is used. Both the abscissa and ordinate in the small panels are labeled in km. (Adapted after Lin and Wang 1996)

- Using an asymptotic method, such as the WKBJ method (e.g., Olver 1997), it is found that an upward propagating internal gravity wave packet in a nonrotating stably stratified fluid would approach the critical level for the dominant frequency and wave number of the packet, but it would not reach the critical level in any finite period of time since along a ray

path, $dz/dt \propto (z - z_c)^2$ as $z \to z_c$, which gives $(t - t_o) \propto 1/(z - z_c)$ as $z \to z_c$ (Bretherton 1966).

This means that it will take an infinite amount of time for a gravity wave packet to reach the critical level.

Thus, the internal wave is physically *absorbed* at the critical level, instead of being either transmitted or reflected, as discussed in the previous section.

In the real atmosphere, a gravity wave is composed by a number of different wave modes which propagate at different phase speeds. This will form a layer of critical levels, i.e. a *critical layer*. This particular type of internal wave behavior in a stratified fluid is illustrated in Fig. 3.13.

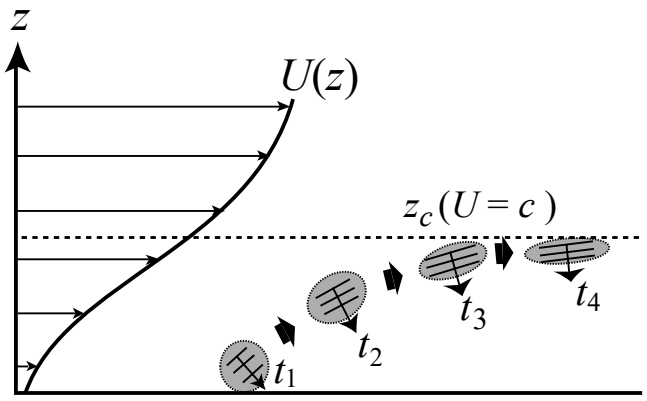

Fig. 3.13: The propagation of a wave packet upward toward a critical level located at $z = z_c$. The particle motions are parallel to the wave crests, which are denoted by straight lines. Note that the vertical wavelength decreases as the wave packet approaches the critical level. The phase lines are horizontally oriented at the critical level in this case. (Adapted after Bretherton 1966)

- When the wave energy associated with a wave packet propagates toward the critical level, the group velocity becomes more horizontal and eventually is oriented completely horizontally in the vicinity of the critical level.

  Near the critical level, the phase velocity is oriented downward since it is itself perpendicular to the group velocity, and fluid parcel motions become horizontal. The vertical wavelength also decreases as the wave packet approaches the critical level.

- In the following discussion for obtaining the solution for (3.7.17), we will assume that the Richardson number, *Ri* ($= N^2/U_z^2$) is always greater than 1/4. *Ri* is also known as the *gradient Richardson number*.

  Near $z = z_c$, $U(z)$ and $N(z)$ may be expanded in power series

$$U(z) = c + U_c'(z - z_c) + \ldots$$
$$N(z) = N_c + N_c'(z - z_c) + \ldots \qquad (3.8.1)$$

  where the prime denotes differentiation with respect to z and the subscript "c" denotes the function value at the critical level (z_c).

We assume that z_c is a *regular singularity* which requires $U'(z_c) \neq 0$. Hence, we seek a solution for (3.7.17) of the form,

$$\hat{w}(z) = \sum_{n=0}^{\infty} a_n (z - z_c)^{n+\alpha}, \quad a_o \neq 0, \; n \text{ is an integer.} \tag{3.8.2}$$

Substituting the above expression into the Taylor-Goldstein equation, (3.7.17), leads to the indicial equation,

$$\alpha^2 - \alpha + Ri_c = 0 \tag{3.8.3}$$

where $Ri_c = \left(N_c / U_c'\right)^2$. The above indicial equation has the following solutions,

$$\alpha = 1/2 \pm i\mu; \quad \mu = \sqrt{Ri_c - 1/4} \tag{3.8.4}$$

Thus, near $z = z_c$, a series solution may be found,

$$\begin{aligned}\hat{w}(z) &\approx A(z - z_c)^{1/2+i\mu} + B(z - z_c)^{1/2-i\mu} \\ &= A\ \exp\left[\left(1/2 + i\mu\right)\left(\ln|z - z_c| + i\ \arg(\text{z-z}_\text{c})\right)\right] + B\exp\left[\left(1/2 - i\mu\right)\left(\ln|z - z_c| + i\ \arg(\text{z-z}_\text{c})\right)\right]\end{aligned}$$

(3.8.5)

where "arg" denotes the argument of a complex number. Both $\hat{w}_A$ and $\hat{w}_B$ (i.e., terms in (3.8.5) with coefficients A and B,

respectively) have a branch point at $z = z_c$. In other words, both $\hat{w}_A$ and $\hat{w}_B$ are not single-valued functions when one winds a circle counterclockwise once around z_c.

For the sake of definiteness, we may choose that branch of the natural logarithm (ln) function for which $\arg(z - z_c) = 0$ when $z > z_c$ and introduce the branch cut from $z = z_c$ along the negative *x*-axis.

Therefore, we obtain

$$\hat{w}_A^+(z) = A\sqrt{|z - z_c|}\exp[i\mu \ln(z - z_c)], \text{ and}$$

$$\hat{w}_B^+(z) = B\sqrt{|z - z_c|}\exp[-i\mu \ln(z - z_c)], \quad \text{for} \quad z > z_c. \qquad (3.8.6)$$

In order to determine the appropriate argument, a small Rayleigh friction term to the *x*-momentum equation (3.5.1) and a small Newtonian cooling term can be added to the thermodynamic energy equation (3.5.4). This gives $\arg(z - z_c) = -\pi\,\mathrm{sgn}(U_c')$ when $z < z_c$.

Substituting the above expression into (3.8.5) yields

$$\hat{w}_A^- = A\sqrt{|z\text{-}z_c|}\exp\left[i\mu\ \ln|z-z_c| - (1/2)\pi i\ \text{sgn}\ U_c' + \mu\pi\ \text{sgn}\ U_c'\right],$$

$$\hat{w}_B^- = B\sqrt{|z\text{-}z_c|}\exp\left[-i\mu\ \ln|z-z_c| - (1/2)\pi i\ \text{sgn}\ U_c' - \mu\pi\ \text{sgn}\ U_c'\right], \text{ for } z < z_c. \quad (3.8.7)$$

Both solutions $\hat{w}_A$ and $\hat{w}_B$ in (3.8.6) and (3.8.7) satisfy (3.7.17) mathematically; however, they have different physical meanings and need to be properly determined. From (3.8.6) and (3.8.7), we have

$$\left|\frac{\hat{w}_A^+}{\hat{w}_A^-}\right| = \exp(-\mu\pi\ \text{sgn}\ U_c'); \quad \left|\frac{\hat{w}_B^+}{\hat{w}_B^-}\right| = \exp(\mu\pi\ \text{sgn}\ U_c'). \quad (3.8.8)$$

For $U_c' > 0$ and low-level forcing, the amplitude of the disturbance generated in the lower layer should decrease as it passes across the critical level into the upper layer. Thus, we must choose $\hat{w}_A$.

The proper solution can be found for other situations as well. Note that the above equation also indicates that the wave energy

is exponentially attenuated through the critical level (Booker and Bretherton 1967).

As mentioned earlier, the vertical wave number increases, and the perturbation velocity becomes increasingly horizontal as one approaches the critical level, because

$$m^2(z) \approx \frac{N^2}{(U-c)^2}. \tag{3.8.9}$$

This implies that $m \to \infty$ as $z \to z_c$. Thus, the vertical Wavelength approaches zero near the critical level. This property is also depicted by Fig. 3.13. In the real atmosphere, a localized disturbance is often composed of many Fourier wave components, each with a different wavelength. Since each Fourier wave component has its own critical level, where $U = c = \omega / k$, an atmospheric layer of finite thickness composed of these critical levels, referred to as the critical layer, is often associated with a localized disturbance.

The flow near a critical level is highly nonlinear, since

a small perturbation in the horizontal velocity field will necessarily exceed the basic horizontal flow velocity in the vicinity of the critical level, in a reference frame moving with the phase speed of the wave.

Thus, linear theories are not accurate in the vicinity of a critical level. Based on numerical simulations of varying the Richardson number, three flow regimes have been found (Breeding 1971).

For $Ri > 2.0$, the interaction between the incident wave and the mean flow is largely similar to that predicted by the linear theory as outlined above. That is, very little of the incident wave energy penetrates through the critical level.

For $0.25 < Ri < 2.0$, a significant amount of the wave energy is reflected, part of which can be predicted by linear theory. This condition represents a balance between the outward diffusion of the added momentum from the incident wave and the rate at which it is absorbed at the critical level.

When Ri falls into this range, some wave energy is also transmitted through the critical level.

For $Ri < 0.25$, wave overreflection is predicted. Note that these regime boundaries could be more accurately defined with more recent and sophisticated numerical models.

When *wave overreflection* occurs, more energy than that associated with the incident wave is reflected back from the critical level, because the flow possesses shear instability (Lindzen and Rosenthal 1983).

In this situation, the wave is able to extract energy and momentum from the basic flow during the reflection process.

If the overreflected waves are in phase with the incident waves, waves may grow exponentially with time by resonance, i.e. the *normal mode instability* exists.

If the overreflected waves are partially in phase with the incident waves, waves may grow algebraically with time by partial resonance, i.e., the *algebraic mode instability* exists.

Under certain conditions, such as an unstable layer containing a critical level and capping a stable layer, a wave duct can exist for mesoscale gravity waves, and wave absorption, transmission, and overreflection may occur at different ranges of *Ri* (see Fig. 4.13 and relevant discussions).

- Figure 3.14 shows the linear, steady state responses to a prescribed heating in the layer below the critical level ($z_c = 0$) of a stably stratified flow with $Ri = 10$ and $Ri = 1$.

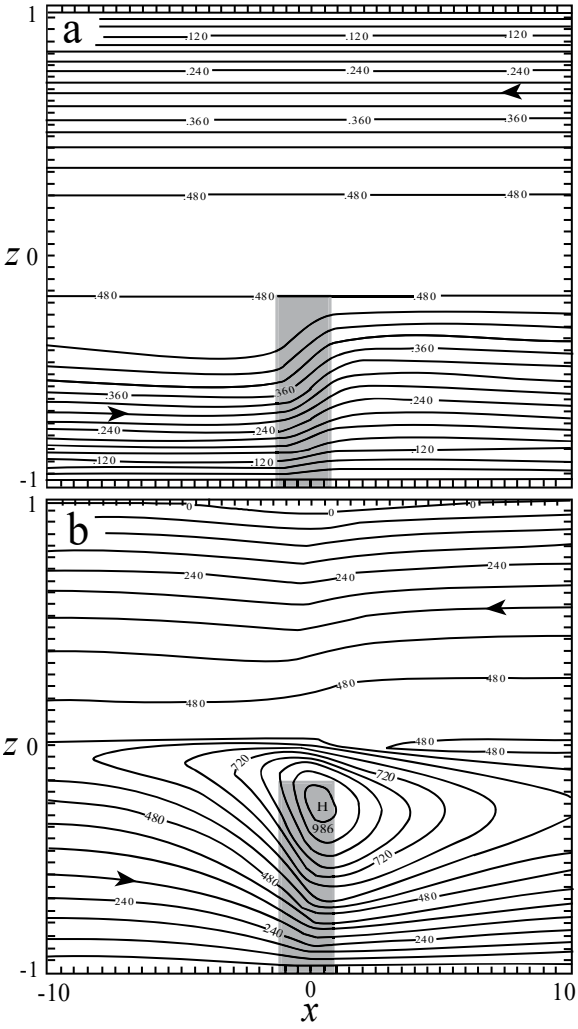

Fig. 3.14: (a) Streamlines for a linear, steady-state stratified airflow over an isolated heat source. The concentrated heating region is shaded. The basic flow has a linear shear (U_z = constant) and its Richardson number (Ri) is 10. (b) Same as (a) except for Ri = 1. All contour values are nondimensionalized. The streamfunction (ψ) used for constructing the streamlines is defined as $u = \partial\psi / \partial z$ and $w = -\partial\psi / \partial x$. (After Lin 1987)

Again, for steady state flow, the critical level coincides with the wind reversal level ($U = 0$).

Upward motion is induced in the vicinity of the heat source, while two regions of very weak compensated downdrafts are produced upstream and downstream from the heat source.

For the case with $Ri = 10$ (Fig. 3.14a), the flow above the critical level is almost undisturbed due to the exponential attenuation associated with critical level absorption.

With $Ri = 1$ (Fig. 3.14b), upstream of the heat source is occupied by subsidence, while downstream of the heat source is occupied by ascending motion. This subsidence occurs due to strong advection (Section 6.2). The disturbance above the critical level is more pronounced because more energy is transmitted through the critical level into the upper layer.

- The critical level dynamics can be extended to a rotating fluid flow.

  In a rotating fluid system, the governing equation for the small-amplitude vertical velocity $w'(t,x,z)$ for a two-dimensional, inviscid, Boussinesq flow on an f plane, can be derived (e.g., Smith 1986) and is given by

$$\frac{D}{Dt}\left(\frac{D^2}{Dt^2}\nabla^2 w' + f^2\frac{\partial^2 w'}{\partial z^2} - U_{zz}\frac{D}{Dt}\frac{\partial w'}{\partial x} + N^2\frac{\partial^2 w'}{\partial x^2}\right) - 2f^2 U_z\frac{\partial^2 w'}{\partial x \partial z} = 0. \qquad (3.8.10)$$

Taking a normal mode approach, substitution of $w' = \hat{w}(z)\exp[ik(x-ct)]$, leads to the following vertical structure equation:

$$\frac{\partial^2 \hat{w}}{\partial z^2} - \frac{2f^2 U_z}{(U-c)[k^2(U-c)^2 - f^2]}\frac{\partial \hat{w}}{\partial z} + \frac{k^2[N^2 - k^2(U-c)^2]}{k^2(U-c)^2 - f^2}\hat{w} = 0. \qquad (3.8.11)$$

The above equation indicates that in addition to the singularity at $U = c$, there are two additional singularities, $U = c \pm f/k$. These additional levels are called *inertial critical levels* (Jones 1967). For incident monochromatic (single wavelength) waves, the inertial critical levels can absorb wave energy in linear flow but tend to reflect wave energy in nonlinear flow (Wurtele *et al*. 1996).

Based on the Richardson number ($Ri = N^2/U_z^2$) and the Rossby number ($R_o = U/fa$, where a is the mountain scale, such as the

half-width of a bell-shaped mountain), four flow regimes for two-dimensional back-sheared flow over an isolated mountain ridge on an *f*-plane can be identified (Shen and Lin 1999):

(I) inertia-gravity wave regime,
(II) mixed inertia-gravity waves and trapped baroclinic lee wave regime,
(III) mixed evanescent wave and trapped baroclinic lee wave regime, and
(IV) transient wave regime with possible nongeostrophic baroclinic instability.

The baroclinic lee wave theory of lee cyclogenesis (Section 5.5) belongs to regime II of moderate R_o and moderate Ri (~ 6.25), or small R_o ($\sim 0.4-0.8$) and moderate (large) Ri (≥ 25). It is also found that three-dimensionality, directional wind shear, and rotation promote horizontal energy dispersion (Shutts 2003).

Appendix 3.1 Derivations of shallow-water equations

Consider a non-rotating, hydrostatic, two-layer fluid system with constant densities ρ_1 and ρ_o in the upper and lower layers, respectively, and assume that $\rho_1 < \rho_o$. Note that the horizontal pressure gradients, $\partial p / \partial x$ and $\partial p / \partial y$, are independent of height in each layer if the fluid system is in hydrostatic balance because

$$\frac{\partial}{\partial z}\left(\frac{\partial p}{\partial x}\right)=\frac{\partial}{\partial x}\left(\frac{\partial p}{\partial z}\right)=-\frac{\partial}{\partial x}(\rho g)=0\,, \tag{A3.1.1}$$

because the density is constant in each layer. We also assume that no horizontal pressure gradients exist in the upper layer. At point A in Fig. 3.2, we have

$$\frac{p-(p+\delta p_1)}{\delta z}=-\rho_1 g\,, \tag{A3.1.2}$$

according to the hydrostatic equation. The above equation leads to

$$p+\delta p_1 = p+\rho_1 g\delta z = p+\rho_1 g\frac{\partial(H+h')}{\partial x}\delta x\,, \tag{A3.1.3}$$

where H is the undisturbed upstream fluid depth and h' the perturbation or the vertical displacement from H, and $\partial(H+h')/\partial x$ is the slope of the interface. Similarly, we may derive the pressure at point B,

$$p+\delta p_2 = p+\rho_o g\delta z = p+\rho_o g\frac{\partial(H+h')}{\partial x}\delta x\,. \tag{A3.1.4}$$

Thus, the horizontal pressure gradient in the x-direction, $\partial p/\partial x$, at the interface can be approximated by

$$\frac{\partial p}{\partial x}=g\Delta\rho\frac{\partial(h+h_s)}{\partial x}, \tag{A3.1.5}$$

where $\Delta\rho=\rho_o-\rho_1$. In deriving (A3.1.5), we have used $h+h_s=H+h'$, where h is the instantaneous depth of the fluid, and h_S is the height of the bottom topography (Fig. 3.2). Similarly, we may derive the horizontal pressure gradient in the y-direction

$$\frac{\partial p}{\partial y}=g\Delta\rho\frac{\partial(h+h_s)}{\partial y}\,. \tag{A3.1.6}$$

Therefore, the horizontal momentum equations become

$$\frac{\partial u}{\partial t} + u\frac{\partial u}{\partial x} + v\frac{\partial u}{\partial y} + w\frac{\partial u}{\partial z} = -g'\frac{\partial (h + h_s)}{\partial x}, \tag{A3.1.7}$$

$$\frac{\partial v}{\partial t} + u\frac{\partial v}{\partial x} + v\frac{\partial v}{\partial y} + w\frac{\partial v}{\partial z} = -g'\frac{\partial (h + h_s)}{\partial y}, \tag{A3.1.8}$$

where $g' = g\Delta\rho / \rho_o$ is called *reduced gravity*. Assuming that initially there is no vertical shear of the horizontal wind velocity ($\partial u / \partial z = \partial v / \partial z = 0$), it can be shown that u and v will be independent of z at any subsequent time. Under this constraint, (A3.1.7) and (A3.1.8) reduce to

$$\frac{\partial u}{\partial t} + u\frac{\partial u}{\partial x} + v\frac{\partial u}{\partial y} = -g'\frac{\partial (h + h_s)}{\partial x}, \tag{A3.1.9}$$

$$\frac{\partial v}{\partial t} + u\frac{\partial v}{\partial x} + v\frac{\partial v}{\partial y} = -g'\frac{\partial (h + h_s)}{\partial y}. \tag{A3.1.10}$$

The above equations give (3.4.1) and (3.4.2) respectively.

Integrating the continuity equation, (2.2.4), from the surface of the bottom topography ($z = h_s$) to the interface ($z = h + h_s = H + h'$) with respect to z leads to

$$\int_{h_s}^{H+h'} \left(\frac{\partial u}{\partial x} + \frac{\partial v}{\partial y} \right) dz + \int_{h_s}^{H+h'} \frac{\partial w}{\partial z} dz = 0, \tag{A3.1.11}$$

because $D\rho / Dt = 0$ in each layer of the fluid. Since u and v are assumed to be independent of z initially, then both $\partial u / \partial x$ and $\partial v / \partial y$ will be independent of z for all time afterwards. Thus, the vertically integrated mass continuity equation, (A3.1.11), reduces to

$$h\left(\frac{\partial u}{\partial x} + \frac{\partial v}{\partial y} \right) + w(z = h + h_s) - w(z = h_s) = 0. \tag{A3.1.12}$$

The vertical velocity is just the rate at which the height is changing:

$w = Dz / Dt = \partial h / \partial t + u\partial h / \partial x + v\partial h / \partial y$. Substituting w into (A3.1.12) leads to

$$h\left(\frac{\partial u}{\partial x}+\frac{\partial v}{\partial y}\right)+\left(\frac{\partial(h+h_s)}{\partial t}+u\frac{\partial(h+h_s)}{\partial x}+v\frac{\partial(h+h_s)}{\partial y}\right)-\left(u\frac{\partial h_s}{\partial x}+v\frac{\partial h_s}{\partial y}\right)=0. \qquad \text{(A3.1.13)}$$

This can be further reduced to the expression

$$\frac{\partial h}{\partial t}+u\frac{\partial h}{\partial x}+v\frac{\partial h}{\partial y}+h\left(\frac{\partial u}{\partial x}+\frac{\partial v}{\partial y}\right)=0 \qquad \text{(A3.1.14)}$$

because h_s, the height of the bottom topography, is generally assumed to be independent of time. Equation (A3.1.14) gives (3.4.3).

References

Baines, P. G., 1995: *Topographic Effects in Stratified Flows.* Cambridge University Press, 482pp.

Bluestein, H. B., and M. H. Jain, 1985: Formation of mesoscale lines of precipitation: Severe squall lines in Oklahoma during the spring. *J. Atmos. Sci.*, **42**, 1711-1732.

Booker, J. R., and F. P. Bretherton, 1967: The critical layer for internal gravity waves in a shear flow. *J. Fluid Mech.*, **27**, 513-539.

Breeding, R. J., 1971: A nonlinear investigation of critical levels for internal atmospheric gravity waves. *J. Fluid Mech.*, **50**, 545-563.

Bretherton, F. P., 1966: The propagation of groups of internal gravity waves in a shear flow. *Quart. J. Roy. Meteor. Soc.*, **92**, 466-480.

Durran, D. R., 1990: Mountain waves and downslope winds. *Atmospheric Processes over Complex Terrain*, Meteor. Monogr., No. **45**, Amer. Meteor. Soc., 59-81.

Emanuel, K., and D. J. Raymond, 1984: *Dynamics of Mesoscale Weather Systems*. Ed. J. B. Klemp, NCAR, 1984.

Hooke, 1986: Gravity waves, in *Mesoscale Meteorology and Forecasting* (P.S. Ray, Ed.), Boston, Amer. Meteor. Soc., 272-288.

Houghton, D. D., and A. Kasahara, 1968: Non-linear shallow fluid flow over an isolated ridge. Comm. *Pure Appl. Math.*, **21**, 1-23.

Jones, W. L., 1967: Propagation of internal gravity wave in fluids with shear and rotation. *J. Fluid Mech.*, **30**, 439-448.

Klemp, J. B., and D. K. Lilly, 1975: The dynamics of wave-induced downslope winds. *J. Atmos. Sci.*, **32**, 320-339.

Lin, Y.-L., 1987: Two-dimensional response of a stably stratified flow to diabatic heating. *J. Atmos. Sci.*, **44**, 1375-1393.

Lindzen, R. S., and A. J. Rosenthal, 1983: Instabilities in a stratified fluid having one critical level. Part III: Kelvin-Helmholtz instabilities as overreflected waves. *J. Atmos. Sci.*, **40**, 530-542.

Long, R. R., 1970: Blocking effects in flow over obstacles. *Tellus*, **22**, 471-480.

Mowbray, D. E., and B. S. H. Rarity, 1967: A theoretical and experimental investigation of the phase configuration of internal waves of small amplitude in a density stratified liquid. *J. Fluid Mech.*, **28**, 1-16.

Nicholls, M. E., and R. A. Pielke Sr., 2000: Thermally induced compression waves and gravity waves generated by convective storms. *J. Atmos. Sci.*, **57**, 3251-3271.

Olver, F. W. J., 1997: *Asymptotics and Special Functions*. A. K. Peters, Ltd., 592pp.

Shen, B.-W., and Y.-L. Lin, 1999: Effects of critical levels on two-dimensional back-sheared flow over an isolated mountain ridge on an f plane. *J. Atmos. Sci.*, **56**, 3286-3302.

Shutts, G., 2003: Inertia-gravity wave and neutral Eady wave trains forced by directionally sheared flow over isolated hills. *J. Atmos. Sci.*, **60**, 593-606.

Smith, R. B., 1979: The influence of mountains on the atmosphere. *Adv. in Geophys*., **21**, Ed. B. Saltzman, Academic Press, NY, 87-230.

Smith, R. B., 1986: Further development of a theory of lee cyclogenesis. *J. Atmos. Sci.*, **43**, 1582-1602.

Sommerfeld, A., 1949: *Partial Differential Equations in Physics*. Academic Press, 335pp.

Turner, J. S., 1973 *Buoyancy Effects in Fluids*. Cambridge University Press, 368 pp.

Wurtele, M. G., A. Data, and R. D. Sharman, 1996: The propagation of gravity-inertia waves and lee waves under a critical level. *J. Atmos. Sci.*, **53**, 1505-1523.

Wyss, J. and K. A. Emanuel, 1988: The pre-storm environment of midlatitude prefrontal squall lines. *Mon. Wea. Rev.,* **116**, 790–794.

Problems

3.1 Using the normal mode approach, derive the Lamb wave solution from (3.3.1), (3.3.2), (3.3.7) and (3.3.8).

3.2 (a) Derive (3.4.10) from (3.4.7)-(3.4.9). (b) Find the dispersion relation for linear, three-dimensional (*x, y, t*) shallow water waves. Are the waves dispersive or not? (c) From (b), find the group velocities, c_{gx} and c_{gy}.

3.3 Consider a two-dimensional, one-layer fluid flow over an obstacle. Estimate the Froude number (F) and nondimensional mountain height (M), assuming $H = 1000$ m, $U = 4$ ms^{-1}, $h_m = 200$ m. What is the flow regime, based on the flow regime diagram for one-layer shallow-water system (Fig. 3.3)? Change flow and/or orographic parameters to shift the above flow regime to the other four flow regimes.

3.4 Show that in the flow regime with $N^2 >> \Omega^2$ the vertical momentum equation reduces to the hydrostatic equation, (3.5.18). Show that the vertical wavelength is $2\pi U/N$ for a steady state flow.

3.5 (a) Assuming $N^2 << \Omega^2$, prove that the vertical momentum equation, (3.5.2), reduces to (3.5.20).

(b) Show that (3.5.21) reduces to (3.5.22) for a flow starting with no vorticity at $t = 0$ (i.e. assume that the flow is initially irrotational).

3.6 Derive (3.6.6) from (3.6.1)-(3.6.5).

3.7 Consider a uniform basic flow, which has a uniform buoyancy frequency $N = 0.012$ s^{-1}, passing over a mountain with a horizontal scale of 20 km. What is the critical basic flow speed that separates the upward propagating waves and evanescent waves, assuming the Earth's rotation can be ignored?

3.8 (a) Derive the group velocities for inertia-gravity waves for $U = 0$.

(b) Derive (3.6.23) for the ratio of c_{gz} / c_{gx}.

3.9 Derive the dynamic interface boundary condition (3.7.13).

3.10 Derive (3.7.17) from (2.2.14)-(2.2.18) by assuming a two-dimensional ($\partial / \partial y = 0, V = 0$), nonrotating, adiabatic, and Boussinesq flow.

Table captions

Table 3.1: A summary of atmospheric waves

Table 3.2: Dispersion relations and approximated equations of *w'* for mesoscale waves in different flow regimes

Figure captions

Fig. 3.1: Propagation of a wave group and an individual wave. The solid and dashed lines denote the group velocity (c_g) and phase velocity (c_p), respectively. Shaded oval denotes the concentration

of wave energy which propagates with the group velocity. The phase speed c_p equals x_i / t_i, where i = 1, 2, or 3. (Adapted after Holton 2004)

Fig. 3.2: A two-layer system of homogeneous fluids. Symbols H, h, h_s, and h' denote the undisturbed fluid depth, actual fluid depth, bottom topography, and perturbation (vertical displacement) from the undisturbed fluid depth, respectively. The densities of the upper and lower layers are ρ_1 and ρ_o, respectively. The pressure perturbations at A and B from p in the upper layer are denoted by $p + \delta p_1$ and $p + \delta p_2$, respectively.

Fig. 3.3: Five flow regimes of the transient one-layer shallow water system, based on the two nondimensional control parameters ($F = U / \sqrt{gH}$, $M = h_m / H$). (a) Regime A: supercritical flow, (b) Regime B: flow with both upstream and downstream propagating hydraulic jump, (c) Regime C: flow with upstream propagating jump and downstream stationary jump, (d) Regime D: completely blocked flow, and (e) Regime E: subcritical flow. The dashed lines in (b) and (c) denote transient water surface. In regimes B and C, upstream flow is partially blocked. (Adapted after Baines 1995 and Durran 1990)

Fig. 3.4: (a) Analysis of potential temperature from aircraft flight data and rawinsondes for the 11 January 1972 Boulder windstorm. The bold dashed line separates data taken from the Queen Air aircraft (before 2200 UTC) and from the Saberliner aircraft (after 0000 UTC) (Adapted after Klemp and Lilly 1975). The severe downslope wind reached a speed greater than 60 ms^{-1}. (b) A sketch of flow Regime C of Fig. 3.3(c), which may be used to explain the phenomenon associated with (a). Q is the volume flux per unit width. (Adapted after Turner 1973)

Fig. 3.5: An internal hydraulic jump associated with a severe downslope windstorm formed along the eastern Sierra Nevada (to the right) and Owens Valley, California. The hydraulic jump was

made visible by the formation of clouds and by dust raised from the ground in the turbulent flow behind the jump. (Photographed by Robert Symons)

Fig. 3.6: The evolution of an initial symmetric wave, which is imagined to be composed of three rectangular blocks with shorter blocks on top of longer blocks. The wave speeds of these fluid blocks are approximately equal to $c_n = \sqrt{g(H + nh)}$, based on shallow-water theory, where n = 1, 2, and 3, H is the shallow-water layer depth, and h is the height of an individual fluid block. The wave steepening in (b) and wave overturning in (c) are interpreted by the different wave speeds of different fluid blocks because $c_3 > c_2 > c_1$.

Fig. 3.7: Vertical oscillation of an air parcel in a stably stratified atmosphere when the Brunt-Vaisala frequency is N. The oscillation period of the air parcel is $\tau_b = 2\pi / N$ and the volume of the air parcel is proportional to the area of the circle. (Adapted after Hooke 1986)

Fig. 3.8: (a) Vertically propagating waves and (b) evanescent waves for a linear, two-dimensional, inviscid flow over sinusoidal topography. (Adapted after Smith 1979)

Fig. 3.9: Basic properties of a vertically propagating gravity wave with $k > 0, m < 0,$ and $\omega > 0$. The energy of the wave group propagates with the group velocity ($\boldsymbol{c_g}$, thick blunt arrow), while the phase of the wave propagates with the phase speed ($\boldsymbol{c_p}$). Relations between w', u', p', and θ' as expressed by (3.5.16) and (3.5.17) are also sketched. Symbols H and L denote the perturbation high and low pressures, respectively, while W and C denote the warmest and coldest regions, respectively, for the wave at t_1. Symbol α defined in (3.5.13) represents the angle of the wave number vector $\boldsymbol{k}$ from the horizontal axis or the wave front (line of constant phase) from the vertical axis. (Adapted after Hooke 1986)

Fig. 3.10: (a) Similar to Fig. 3.9, except for a hydrostatic inertia-gravity wave with $m < 0$, $k > 0$, l = 0, $\omega > 0$, and $f > 0$. Meridional (i.e. north-south) perturbation wind velocities (v') are shown by

arrows pointed into and out of the page. (b) The projection of fluid particle motion associated with a hydrostatic inertia-gravity wave onto the horizontal plane is an ellipse with ω/f as the ratio of major and minor axes. The velocity vector associated with a plane inertia-gravity wave rotates anticyclonically in the Northern Hemisphere with height for upward energy propagation. (Adapted after Hooke 1986)

Fig. 3.11: Examples of wave reflection in a stratified flow with a piecewise constant profile in Brunt-Vaisala frequency (N). Case ω_1 has wave solutions in both layers; Case ω_2 (wave reflection case) has wave solutions in the lower layer, evanescent solutions in upper layer; and Case ω_3 has evanescent solutions in both layers.

Fig. 3.12: Wave reflection in a continuously stratified fluid. N and T are the Brunt-Vaisala frequency and temperature of the sounding, respectively, and ω is the wave frequency. Ray paths are reflected at the reflection level at which $\omega = N$. A wave packet is also depicted in the figure. The short blunt arrows and long thin arrows denote the group and phase velocities, respectively, of the wave packet. Particle motions are parallel to the constant phase lines or wave fronts, which become vertically oriented at the reflection level since α, defined in (3.5.13) and also illustrated in Fig. 3.9, approaches 0. (Adapted after Hooke 1986)

Fig. 3.13: The propagation of a wave packet upward toward a critical level located at $z = z_c$. The particle motions are parallel to the wave crests, which are denoted by straight lines. Note that the vertical wavelength decreases as the wave packet approaches the critical level. The phase lines are horizontally oriented at the critical level in this case. (Adapted after Bretherton 1966)

Fig. 3.14: (a) Streamlines for a linear, steady-state stratified airflow over an isolated heat source. The concentrated heating region is shaded. The basic flow has a linear shear (U_z = constant) and its Richardson number (Ri) is 10. (b) Same as (a) except for $Ri = 1$. All contour values are

nondimensionalized. The streamfunction (ψ) used for constructing the streamlines is defined as $u = \partial\psi / \partial z$ and $w = -\partial\psi / \partial x$. (After Lin 1987)